Colloids and Surfaces A 530 (2017) 164–171

Contents lists available at ScienceDirect

Colloids and Surfaces A

journal homepage: www.elsevier.com/locate/colsurfa

Silica coated LSMO magnetic nanoparticles for the pH-Responsive delivery of 5-Fluorouracil anticancer drug

C.O. Ehi-Eromosele[a,*], B.I. Ita[a,b], E.E.J. Iweala[c]

[a] Department of Chemistry, Covenant University, PMB 1023, Ota, Nigeria
[b] Department of Pure and Applied Chemistry, University of Calabar, Calabar, Nigeria
[c] Department of Biological Sciences, Covenant University, PMB 1023, Ota, Nigeria

GRAPHICAL ABSTRACT

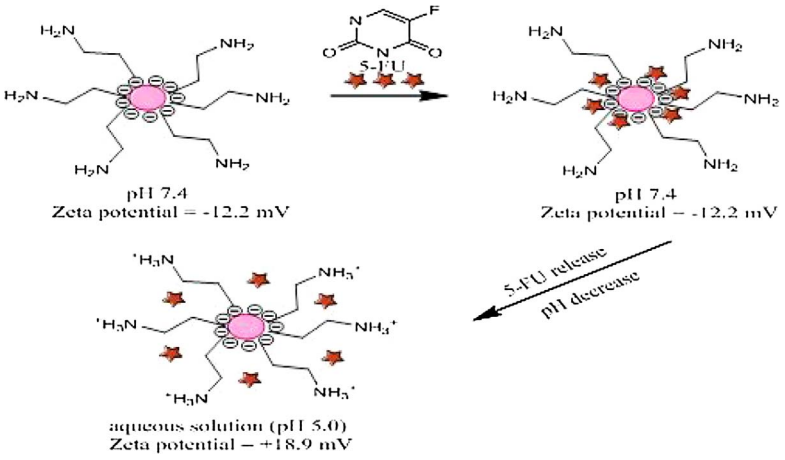

ARTICLE INFO

Keywords:
pH-responsive
Magnetic nanoparticles
Silica
5-Fluorouracil
Drug delivery

ABSTRACT

The design of a drug delivery system capable of a pH-responsive controlled 5-fluorouracil anticancer drug release to cancer sites is one of the important options to reduce the well documented side effects of this drug. $La_{0.7}Sr_{0.3}MnO_3$ (LSMO) magnetic nanoparticles (MNPs) were synthesized by solution combustion synthesis and the optimized MNPs were coated with silica. X-ray diffraction patterns reveal that the crystal structure is a single perovskite phase which was unchanged after silica coating. Silica coating on LSMO was found to reduce the nanoparticle crystallite and magnetic properties. The silica surface of LSMO MNPs was functionalized to confer a pH-dependent switchable surface and was used to demonstrate the pH-responsive controlled release of 5-FU anticancer drug which was significantly higher than the 5-FU released from silica coated LSMO MNPs that were not functionalized. The *in-vitro* release studies show that only 11.36% of 5-FU was released at pH 7.4 (mimic of the physiological environment) and 37.20% at pH 5.0 (mimic of the intracellular organelles of cancer cells). The pH-responsive release of this functionalized silica coated LSMO MNPs suggest that it could be used in the controlled release of 5-FU anticancer drug at tumor sites.

* Corresponding author.
E-mail address: cyril.ehi-eromosele@covenantuniversity.edu.ng (C.O. Ehi-Eromosele).

http://dx.doi.org/10.1016/j.colsurfa.2017.07.059
Received 27 May 2017; Received in revised form 18 July 2017; Accepted 19 July 2017
Available online 21 July 2017

1. Introduction

Many anticancer drugs exhibit poor aqueous solubility, low bioavailability, low selectivity and non-specificity which often limit their clinical use. As a result, research has been focused on the development of drug delivery systems (DDS) capable of not only a sustained and a controlled release of its cargo at diseased sites but also incorporating a targeting moiety. Such additional functionalities in a DDS will enhance the efficacy of anticancer drugs and reduce their associated side effects. DDS can use the passive and active targeting mechanisms to deliver their cargoes to diseased sites. Magnetic nanoparticle-based anticancer DDS, for example, are accumulated and retained in the cancerous extracellular matrix through leaky blood vessels at the cancer sites, the so called enhanced permeation retention effect. After systemic administration and increased half-life in the blood circulation, well-defined magnetic nanoparticle-based DDS can reach and be retained in the cancer sites also benefiting from the passive targeting effect [1,2]. To further improve drug delivery to cancerous site and invariably reduce side effects, smart nano-vectors are being developed capable of charge reversal in response to external stimuli such as pH [3–5] for the controlled release of their payloads at cancerous site (active targeting effect).

Amongst the common drug solubilisation strategies used in the pharmaceutical industry, nano-delivery systems have been the most promising [6]. In this regard, magnetic nanoparticles (MNPs) have attracted great interest due to their inherent magnetic properties and biocompatibility [7]. The use of MNPs in targeted drug delivery triggered by pH change and magnetic activation has been demonstrated [3,8–10]. The unique physico-chemical properties of MNPs coupled with their sensing, moving and heating capabilities have made them to be amenable in biomedical applications such as targeted drug delivery, magnetofection, hyperthermia, etc. Naturally, superparamagnetic iron oxides nanoparticles have been the most popular formulations used in biomedical applications because of its ease of synthesis, high biocompatibility and easy functionalization. However, there has been an increasing interest in the use of lanthanum manganese perovskite (LSMO) materials for biomedical applications due to their tunable Curie temperature, biocompatibility and superparamagnetic nature [11].

5-fluorouracil (5-FU) is an effective anticancer drug available for the treatment of a variety of solid cancers such as stomach, colon, lung and breast cancer [12–15]. 5-FU is usually given intravenously because of the problems associated with its oral administration. The intravenous route of administration is associated with problems such as toxic side effects on the bone marrow and gastrointestinal tract and its low selectivity [16,17]. Also, 5-FU is sparingly soluble in water [18]. In order to overcome these limitations, nanoparticle based stimuli responsive delivery systems are being exploited for the controlled release of 5-FU to cancerous site.

Herein, we report the development of a pH responsive functionalized silica coated MNPs that is capable of triggered intracellular 5-FU release as a result of charge reversal at the lower pH in cancer cells to enhance the release of 5-FU drug. Porous silica was chosen for the surface modification of the LSMO MNPs because of their large, easily tunable surface and biocompatibility. The silica surface was covalently functionalized with (3-Amino propyl)triethoxysilane to confer a charge reversal (switchable surface) in response to pH. The silanol groups would be ionized, at pH 7.4 (physiological environment), to be more negatively charged which aids the increased entrapment of positively charged 5-FU drug. While at pH 5 (intracellular organelles of cancer cells) there is a charge conversion due to increased protonation of the amine groups and diminished silanol ionization thereby, facilitating the escape of the entrapped 5-FU drug at cancerous site where its activity is needed.

2. Experimental

2.1. Materials

All chemical reagents namely lanthanum nitrate, strontium nitrate, manganese nitrate, citric acid monohydrate, tetraethoxy silane (TEOS), ethanol, ammonia solution (ammonium hydroxide solution, ca 25% NH_3) and (3-Amino propyl)triethoxysilane (APTES) were obtained from Sigma Aldrich. 5-Fluorouracil was obtained from Alfa Aesar, UK. Double distilled water was used throughout the experiments. All the solvents and other materials used were of analytical grade and were used without further purification.

2.2. Synthesis of LSMO cores

$La_{0.7}Sr_{0.3}MnO_3$ (LSMO) MNPs were prepared by the solution combustion method using citric acid as fuel. The optimization of the particle size, crystallinity and magnetisation of LSMO MNPs using different citric acid to nitrate ratios have been reported elsewhere [19]. The fuel rich LSMO sample was selected since it presented a pure LSMO phase and a comparatively high saturation magnetization.

2.3. Surface coatings of LSMO MNPs

The following LSMO MNPs were coated with silica by the modified Stober method [20]. The dried MNPs (100 mg) were added to ethanol solution (150 mL) that had distilled water (10 mL) and ammonium hydroxide (2 mL) and the solution was sonicated for 1 h. Then, TEOS (2 mL) was added to the solution and sonicated for 15 min with this process repeated twice. Finally, the mixture was allowed to stand for 24 h. The solution was filtered and the MNPs were washed with ethanol five times and dried at 60 °C in the oven to obtain LSMO-SiO_2.

2.4. APTES functionalisation of LSMO-SiO_2

The functionalization of LSMO-SiO_2 with APTES was done according to the method described elsewhere [21]. LSMO-SiO_2 (30 mg) was dispersed in acetonitrile by sonication. 100 μL APTES was added to the dispersion and was refluxed at 85 °C for 24 h to yield aminopropyl functionalized silica coated LSMO MNPs. The precipitate was then centrifuged and washed once with acetonitrile and thrice with hot methanol (40 °C) before drying it at 60 °C for 45 mins to obtain LSMO-SiO_2-NH_2.

2.5. 5-FU loading and release studies

5-FU stock solution (0.2 mg/ml) was prepared in 0.1 M PBS buffer of pH 7.4. Accurately weighed LSMO-SiO_2-NH_2 (1 mg) MNPs were dispersed in 5-FU stock solution (1 mL). The dispersion was stirred for 12 h in the dark using a bath sonicator. After loading, LSMO-SiO_2-NH_2 MNPs were washed twice with PBS buffer (pH 7.4). All washings were collected and the amount of 5-FU were quantified from UV–vis absorption at 266 nm [21,22]. To measure the amount of 5-FU loaded, calibration curves were done at pH 7.4. The entrapment efficiency (EE) was calculated as follows (Eq. 1). Same procedure was followed for the 5-FU loading of LSMO-SiO_2.

$$EE(\%) = \frac{amount\ \ ofdrug\ loaded\ in\ LSMO - SiO2 - NH2}{Total\ charged\ amount\ of\ 5 - FU} \times 100 \quad (1)$$

To study the controlled release of 5-FU from the loaded MNPs, 1 mg of 5-FU loaded LSMO-SiO_2-NH_2 MNPs was dispersed in 1 mL of 0.1 M PBS buffer (pH 7.4 and pH 5.0) using a bath sonicator. At 4 h intervals, the released amounts of 5-FU were determined by recording the absorbance of 500 μL aliquots of supernatant taken using UV–vis spectroscopy with the withdrawn aliquot added to the test tube. All the release studies were performed at room temperature. Same procedure

was followed for the release studies of 5-FU loaded LSMO-SiO_2.

2.6. Characterisation

XRD was used to identify the structure and phase of the nanoparticles. The X-ray diffractograms of the annealed powders were done at room temperature using a D8 Advance Bruker diffractometer with Cu-Kα radiation source at λ = 0.15406 nm in the 2θ scan range between 10° and 80° at 40 kV, 40 Ma. The X-ray line broadening diffraction peak (110) was employed to calculate the mean crystallite size (D) of the MNPs using the Scherrer formula:

$$D = \frac{0.9\lambda}{\beta Cos\theta}$$

where β is equal to the spectral breadth of the line broadening of the (110) peak measured at half of the height of the peak, θ is the Bragg angle and λ is the radiation wavelength of X-ray used. The surface morphological images and elemental composition of the synthesized NPs were obtained using field emission scanning Electron Microscopes (Nova Nano SEM 600, FEI Co., Netherlands). The silica coating was investigated by using Fourier Transform Infrared spectroscopy (ALPHA, Bruker) in the range of 400–4000 cm^{-1}. Magnetic measurements of the bare and silica coated MNPs were done at room temperature using a Vibrating Scanning Magnetometer (Lake Shore cryotronics-7400 series). Colloidal stability studies of the uncoated and silica coated MNPs in water and in PBS were done using a zetasizer Nano Zs (Malvern instruments). Triple measurements of each sample were done for the Zeta potential at 30 electrode cycles.

3. Results and discussion

3.1. Coating of LSMO MNPs with silica and aminopropyl functionalisation of LSMO-SiO_2

Silica was selected for the coating of LSMO MNPs because unlike polymers, it does not change porosity or swelling in relation to pH changes and it is not susceptible to microbial attack [23]. Also, silica coatings on nanoparticles provide a rich surface chemistry, high biocompatibility and an anomalously high stability, especially in aqueous media. The silica surface (LSMO-SiO_2) was covalently functionalized with APTES to confer charge reversal on the MNPs to yield LSMO-SiO_2-NH_2. The schematic of the silica coating of LSMO MNPs and the aminopropyl functionalisation of the silica surface is shown in Fig. 1.

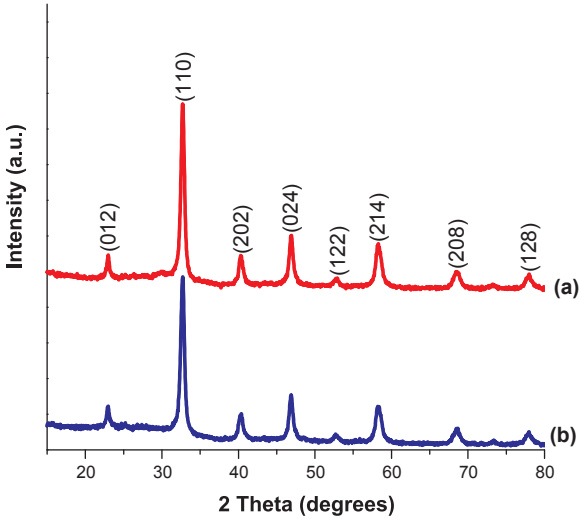

Fig. 2. XRD of (a) uncoated and (b) silica coated nanocrystalline LSMO powders.

3.2. X-ray diffractometry of silica coated LSMO MNPs

XRD was performed on the silica coated sample of nanocrystalline LSMO powder and the diffraction pattern is shown in Fig. 2. The diffraction peaks of the silica coated sample, like the uncoated sample, gave characteristic peaks of rhombohedral perovskite structure R-3c (167) space group. The results showed that the silica coated sample retained the perovskite structure but with a slight suppression of diffraction peaks. Therefore, the XRD data suggests that the silica shell consists mainly of amorphous phase rather than polycrystalline one [24] since there is the absence of silica-derived diffraction peaks.

The crystallite size obtained for the silica coated sample (35 nm) was slightly lower than the uncoated sample (36 nm). A reduction in crystallite size was also recorded for silica coated $CoFe_2O_4$ [25]. This reduction might be due to a lesser agglomeration due to silica coating. The diffraction peaks of all the samples were quite broad, indicating their nanocrystallinity.

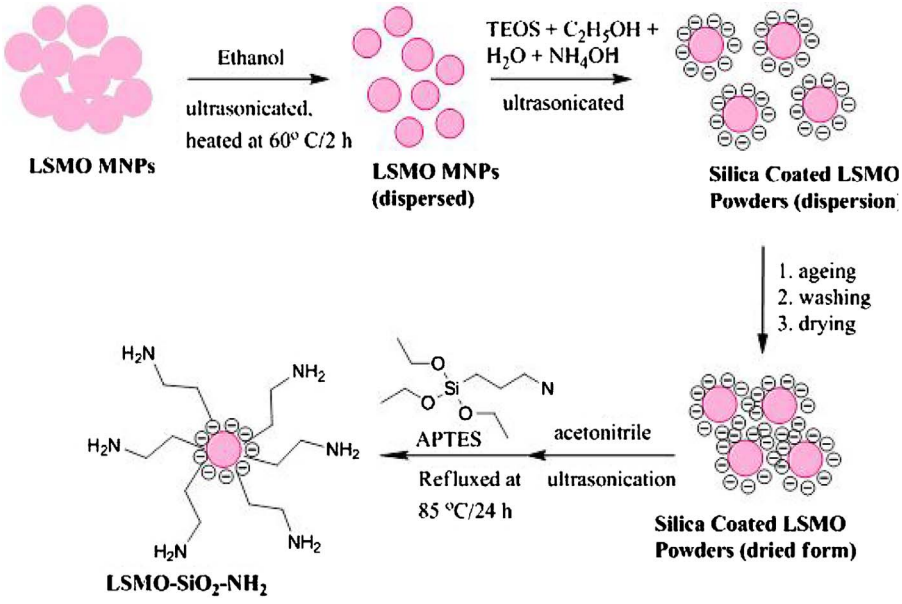

Fig. 1. Schematic of silica coating of LSMO MNPs and aminopropyl functionalization of LSMO-SiO_2.

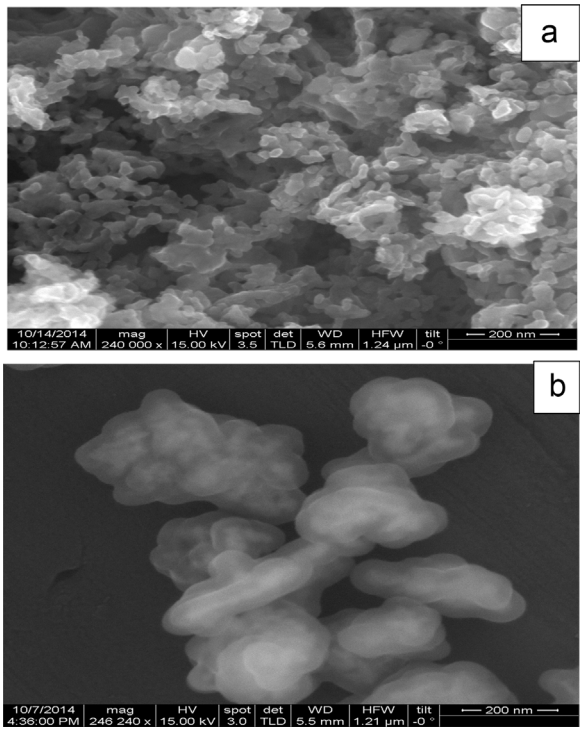

Fig. 3. FESEM images of LSMO powders (a) uncoated (b) silica coated.

3.3. Morphological and chemical composition analysis of silica coated LSMO sample

The FE-SEM images of uncoated and silica coated LSMO MNPs is given in Fig. 3a–b, respectively. There is a reduction in the particle agglomeration as seen in the image of the coated sample in relation to the uncoated sample. The reduced agglomeration confirms the presence of silica coating on the MNPs which helps to reduce the magnetic interactions between NPs and gives a fair homogeneous particle size distribution. The MNPs after silica coatings gives a core-shell like configuration with LSMO MNPs as the core and the silica as the shell (indicated as lighter contours enveloping the MNPs). It can be seen that the LSMO particles were coated with silica. Silica coating of LSMO aids in preventing antigenical effects which could occur as a result of the potential recognition of LSMO surfaces by macrophages that clears the particles from the system, thereby preventing the MNPs from reaching the tumour sites [22].

3.4. Magnetic studies of silica coated LSMO sample

The magnetization loops of the uncoated and silica coated LSMO samples measured at room temperature are shown in Fig. 4. The magnetic parameters including the saturation magnetisation (M_s), remnant magnetization (M_r), coercivity (H_c) and squareness of the loop (M_r/M_s) of the uncoated and coated sample have been extracted from the magnetization loop and are given in Table 1. It can be seen that the applied magnetic field of 20, 000 G was not sufficient to saturate the magnetic moments in the coated sample in its direction, like the uncoated sample. The saturation magnetization of the coated sample (7 emu/g) is smaller compared to the uncoated sample (11 emu/g). The presence of silica coatings that is non-magnetic might account for the reduction in magnetization seen in the coated sample. The silica coatings help to reduce the energy associated with exchange coupling and the particle–particle interaction and therefore reduc the magnetization [26]. The reduction in magnetization might also be due to the lesser amount of magnetic substance per gram in the silica coated sample compared with the uncoated sample [27]. Lesser M_r and M_r/M_s values

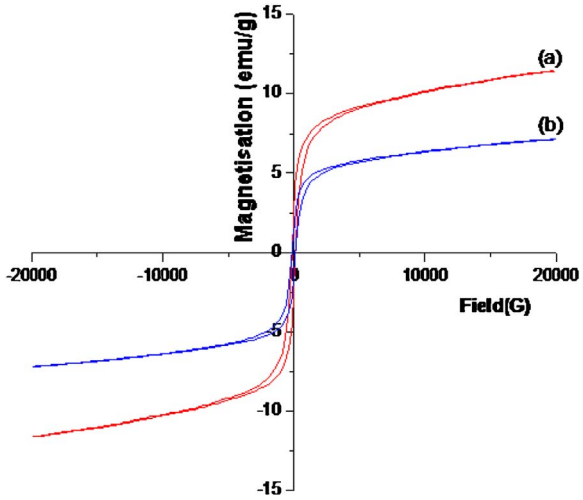

Fig. 4. Magnetic loops of LSMO for (a) the uncoated sample (b) silica coated sample.

Table 1
Magnetic Properties of Silica Coated LSMO MNPs.

Sample	Saturation Magnetisation, M_s (emu/g)	Remanence Magnetisation, M_r (emu/g)	Coercivity (Gauss)	M_r/M_s
Uncoated sample	11	4.20	34	0.38
Silica coated sample	7	1	37	0.14

were recorded for the coated sample but a higher H_c values than the uncoated sample. Very low M_r and H_c were recorded for both the uncoated and coated samples highlighting their near superparamagnetic nature. The silica coated LSMO MNPs gave a saturation magnetization that is required for biomedical applications which should be at least 7–27 emu/g [3].

3.5. Infrared analysis of silica coated LSMO (LSMO-SiO_2) and aminopropyl functionalisation of LSMO-SiO_2 (LSMO-SiO_2-NH_2) samples

The FTIR spectra of uncoated, LSMO−SiO_2 and LSMO−SiO_2−NH_2 samples are shown in Fig. 5a–c, respectively. In the uncoated sample (Fig. 5a), the band around 578 cm^{-1} corresponds to Mn−O vibrations characteristic of perovskite structure [28]. The spectra of carbon associated functional groups, particularly carboxyl groups, appear in 1000–2500 cm^{-1} region [29]. These bands might be due to traces of the unburnt fuel (citric acid) used in the synthesis of the sample. It has been reported that higher temperatures than 1000 °C are required to remove all these carbons associated with the synthesis of LSMO MNPs [30]. Free carbon or carbonates can result from the degradation of citrates if lower calcination temperature is employed. The peaks at 1450 cm^{-1} and 2337 cm^{-1} are due to C=O vibrations which can be related to traces of carbonate [29]. The two peaks at 850 cm^{-1} and 1450 cm^{-1} are due to $SrCO_3$ [29]. The peak at 1450 cm^{-1} is due to C−O bond asymmetric stretching mode while the peak at 850 cm^{-1} corresponds to the in plane bending CO_3^{2-}.

In the case of LSMO-SiO_2, the FTIR spectrum (Fig. 5b) shows all the significant vibrations relevant to silica. Vibrations at 449 cm^{-1} and 1075 cm^{-1} correspond to Si-O-Si bending and stretching, respectively [31,32]. The band at 946 cm^{-1} can be assigned to silanol groups [33] while the one at 798 cm^{-1} is due to Si−O−Si bending vibrations [34,35]. It can be seen that the Mn−O vibrations observed at 578 cm^{-1} in the uncoated sample, appeared at 569 cm^{-1} indicate the presence of the perovskite structure and silica coatings. In the case of the FTIR

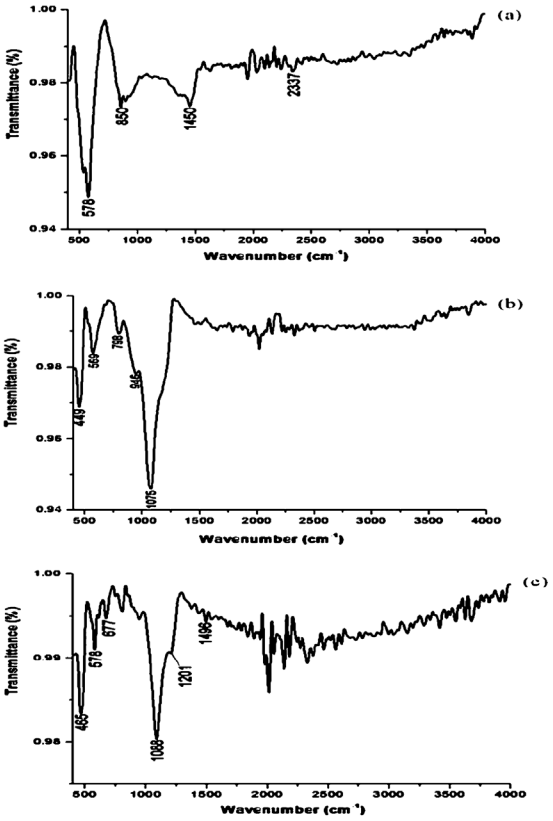

Fig. 5. FTIR spectra of (a) uncoated LSMO (b) LSMO-SiO_2 (c) LSMO-SiO_2-NH_2.

spectrum of LSMO—SiO_2—NH_2 (Fig. 5c), vibrations at 677 cm^{-1} and 1496 cm^{-1} are due to the amino groups stretching and bending vibrations. The absorption peaks in the region of 2800–3025 cm^{-1} can be assigned to the stretching vibrations of methylene groups at LSMO—SiO_2—NH_2. The absorption peak at 1201 cm^{-1} corresponds to the symmetric deformation vibrations of $SiCH_3$. This peak is missing for LSMO—SiO_2, confirming the incorporation of amino-propyl to silica surface.

3.6. Zeta potential studies of LSMO-SiO_2 and LSMO-SiO_2-NH_2

The pH dependent zeta potential of LSMO-SiO_2 and LSMO-SiO_2-NH_2 samples is shown in Fig. 6. The zeta potential distribution of uncoated, LSMO-SiO_2 and LSMO-SiO_2-NH_2 samples using distilled water as a dispersant were 2.4 mV, −7.45 mV and 7.82 mV, respectively. In aqueous environment, the silanol groups ionize to become negatively charged [36] while LSMO-SiO_2-NH_2 will become positively charged as a result of protonation. The uncoated sample showed a lesser zeta potential (2.4 mV) than the coated sample (−7.45 mV) indicating a lesser aggregation of the coated samples in water when compared with the uncoated sample. It is known that colloidal stability increases with increasing zeta potential values. Fig. 6 shows that LSMO-SiO_2-NH_2 sample exhibited charge reversal with respect to pH. At pH 7.4, it shows a negative potential of −12.2 mV which changed to a positive value (+18.9 mV) at pH 5. On the other hand, zeta potential shows no charge reversal for LSMO-SiO_2. It shows a change only in the negative regime from −19.4 mV at pH 7.4 to −6.92 mV at pH 5. As it has been stated earlier, the negative charge comes from the ionization of the silanol groups [36]. At a pH of 7.4, there would be an increase in the ionization of the silanol groups resulting in increased negative charges in the sample. At pH 5, the silanol ionization is lesser thus lowering the net negative charge. At pH 7.4, the surface of LSMO-SiO_2-NH_2 is less negative (−12.2 mV) than that of LSMO-SiO_2 (−19.4 mV). As the pH is reduced to 5, the surface becomes positive (+18.9 mV) due to increased protonation of the amine groups and decreasing silanol ionisation. The colloidal stability is also enhanced at pH 5 indicating its potential to be used as a vector in a drug delivery system. The existence of the acidic environment (pH 6) at the cancerous extracellular matrix would help LSMO-SiO_2-NH_2 to acquire positive charge which is essential for its cellular entry through electrostatic interactions with negatively charged cell wall. Inside the cell, the endosomal pH is even more acidic (pH 5) which makes LSMO-SiO_2-NH_2 MNPs more positive [21]. Acquisition of strong positive charge by LSMO-SiO_2-NH_2 MNPs is expected to facilitate the release of positively charged anti-cancer drugs such as 5-FU.

3.7. 5-FU loading and release studies

Drug loading and release behaviour are the most important characteristics when evaluating a drug delivery system [37]. Fig. 7 gives the schematic diagram of the drug loading and release of LSMO-SiO_2-NH_2 MNPs. An anticancer drug (5-FU) was loaded onto the LSMO-SiO_2-NH_2 MNPs and was held electrostatically. Loading of 5-FU was done at pH 7.4 and at room temperature. At this pH, LSMO-SiO_2-NH_2 is negatively charged (−12.20 mV) and 5-FU is positively charged (pK_a ~8) leading to high entrapment efficiency of ~88%. 5-FU pH dependent release profile was studied by incubating the 5-FU loaded LSMO-SiO_2-NH_2 MNPs for 24 h at room temperature. Fig. 8 shows the 5-FU release

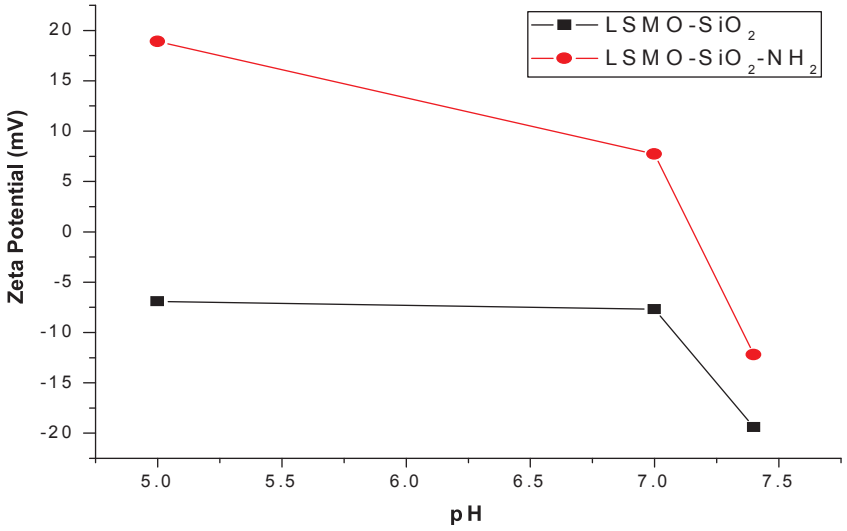

Fig. 6. Zeta potential dependence of pH for LSMO-SiO_2 and LSMO-SiO_2-NH_2 samples.

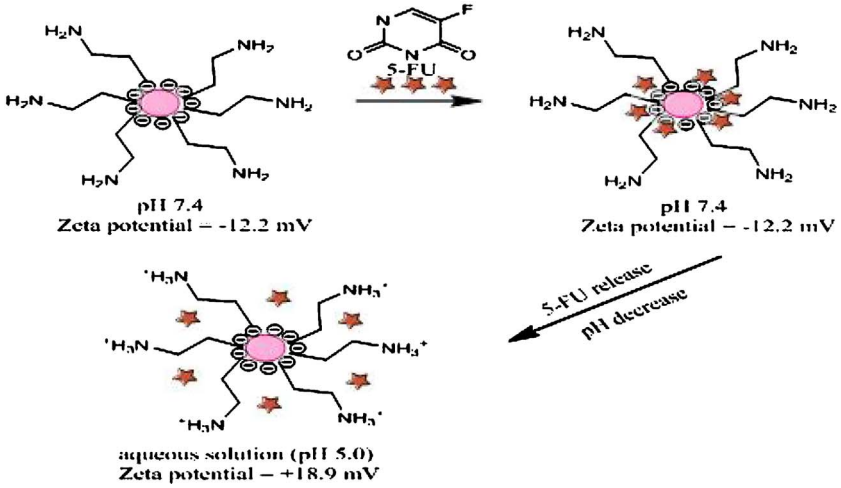

Fig. 7. Schematic of 5-FU drug loading and release of LSMO-SiO_2-NH_2 MNPs.

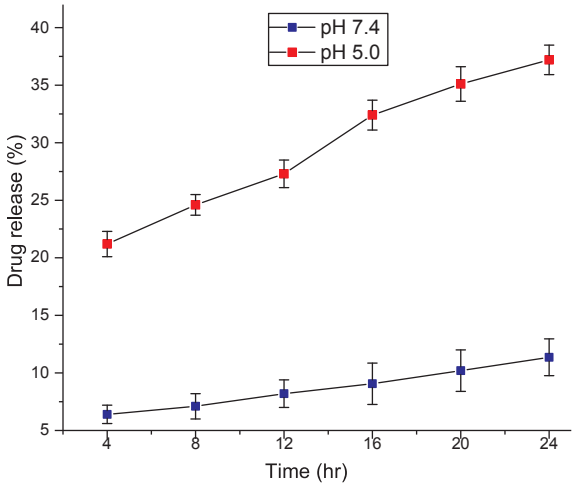

Fig. 8. 5-FU release profiles from LSMO-SiO_2-NH_2 at different pHs.

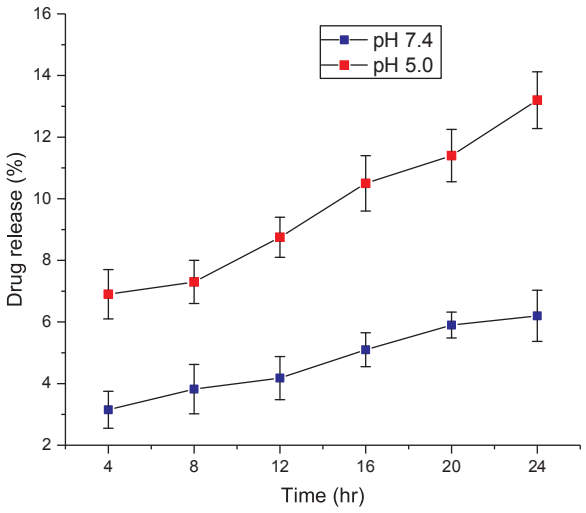

Fig. 9. 5-FU release profiles from LSMO-SiO_2 at different pHs.

profile at pH 5.0 and 7.4. A high release of 5-FU (37.20% in 24 h) is shown by LSMO-SiO_2-NH_2 at pH 5.0 (endosomal pH) due to the repulsive interaction between the positively charged drug and positive LSMO-SiO_2-NH_2 (+18.90 mV). In normal extracellular pH (i.e. 7.4), a low release (11.36%) was observed due to the electrostatic interaction between the positively charged drug and negatively charged LSMO-SiO_2-NH_2. The results clearly show that the release of 5-FU from 5-FU loaded LSMO-SiO_2-NH_2 MNPs is pH-triggered.

The release studies of 5-FU from LSMO-SiO_2 was done to compare its efficacy with that of LSMO-SiO_2-NH_2, and the result is given in Fig. 9. 5-FU was loaded to LSMO-SiO_2 at pH 7.4 with an entrapment efficiency of 92%. The increase in entrapment efficiency, compared to LSMO-SiO_2-NH_2, might be due to the higher electrostatic attraction between the drug and LSMO-SiO_2 having a higher negative charge of −19.40 mV. Release profile for LSMO-SiO_2 showed that maximum release of 5-FU was at pH 5.0 which is about 13.20% after 24 h while a maximum release "of 6.20%" was observed at pH 7.4. The release profile is consistent with the zeta potential values where LSMO-SiO_2 at pH 5 (−6.92 mV) is expected to be less bound to 5-FU than at pH 7.4 (−19.40 mV) hence recording a higher release of 5-FU. Conversely, LSMO-SiO_2 recorded a lesser release of 5-FU at both pH values than LSMO-SiO_2-NH_2. At pH 7.4, LSMO-SiO_2 recorded a higher negative potential making it more bound to 5-FU electrostatically. At pH 5.0, LSMO-SiO_2-NH_2 recorded a higher release of 5-FU than LSMO-SiO_2 because of the charge reversal that released 5-FU by electrostatic repulsion. The high entrapment efficiency and the pH-sensitive release of 5-FU imply that LSMO-SiO_2-NH_2 is a potential delivery system for 5-FU anticancer drug. To our knowledge, there is no report in the literature that has dealt with the use of LSMO MNPs as a delivery vehicle for 5-FU anticancer drug. Table 2 summarises the surface charges, entrapment efficiency and 5-FU releases at different pH for LSMO-SiO_2-NH_2 and LSMO-SiO_2.

The calibration curve made from known concentrations of 5-FU was used to calculate the amount of 5-FU released. Fig. 10 shows a UV–vis spectra of the 5-FU in calibration solutions and Fig. 11 shows the calibration curve for 5-FU.

4. Conclusion

$La_{0.7}Sr_{0.3}MnO_3$ (LSMO) MNPs were synthesized by the solution combustion synthesis and the optimized MNPs were coated with silica which was subsequently used as a drug delivery system. Silica coatings with improved surface area and high specific volume were utilized for the loading of 5-FU. Furthermore, silica surface of LSMO MNPs was functionalized with APTES which conferred a switchable surface in response to pH which was not observed with the silica coated LSMO MNPs. The charge reversal of the designed system from negative to positive as pH varied from 7.4 to 5.0 was used for the effective release of the loaded 5-FU anticancer drug at endosomal pH 5.0. The high entrapment efficiency and the pH-sensitive release of 5-FU imply that LSMO-SiO_2-NH_2 could be employed as a promising controlled 5-FU drug delivery system thereby helping to reduce the well documented side effects of this drug. However, further work needs to be done

Table 2
Summary of the Surface Charge Variation, Entrapment Efficiency and Release of 5-FU for Both LSMO-SiO_2-NH_2 and LSMO-SiO_2 with Respect to pH.

	LSMO-SiO_2-NH_2		LSMO-SiO_2	
	pH 7.4	pH 5.0	pH 7.4	pH 5.0
Surface Charge	−12.20 mV	+18.90 mV	−19.40 mV	−6.92 mV
Entrapment Efficiency	88.00 ± 0.95%	–	92 ± 2.10%	–
Release after 24 h	11.36 ± 1.60%	37.20 ± 1.28%	6.20 ± 0.83%	13.20 ± 0.92%

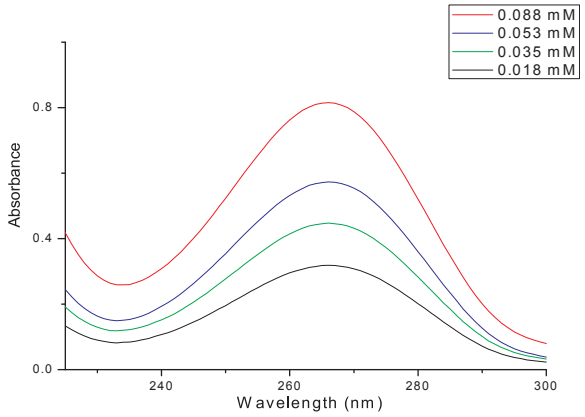

Fig. 10. UV–visible spectra of 5-FU in calibration solutions.

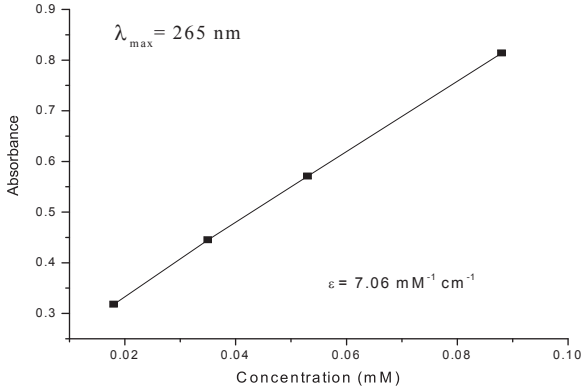

Fig. 11. Linear calibration plot of 5-FU in 0.1 M PBS.

concerning the drug release studies to clarify the effects of ionic strength, types of ions, proteins, metabolites and other molecules before it can be fully implemented in physiological environment.

Acknowledgment

The author, Ehi-Eromosele C.O. appreciates the visiting research award granted by ICMS, Jawarharlal Nehru Center for Advanced Scientific Research, Bangalore, India.

References

[1] H. Gao, T. Cheng, J. Liu, C. Yang, L. Chu, Y. Zhang, R. Ma, L. Shi, Self-regulated multifunctional collaboration of targeted nanocarriers for enhanced tumor therapy, Biomacromolecules 15 (2014) 3634–3642.
[2] S. Manchun, K. Cheewatanakornkool, C.R. Dass, P. Sriamornsak, Novel pH responsive dextrin nanogels for doxorubicin delivery to cancer cells with reduced cytotoxicity to cardiomyocytes and stem cells, Carbohydr. Polym. 114 (2014) 78–86.
[3] Z. Karimi, S. Abbasi, H. Shokrollahi, Gh. Yousefi, M. Fahham, L. Karimi, O. Firuzi, Pegylated and amphiphilic chitosan coated manganese ferrite nanoparticles for pH-sensitive delivery of methotrexate: synthesis and characterization, Mater. Sci. Eng. C (2016).
[4] L. Han, J. Zhao, X. Zhang, W. Cao, X. Hu, G. Zou, X. Duan, X.-J. Liang, Enhanced siRNA delivery and silencing gold-chitosan nanosystem with surface charge-reversal polymer assembly and good biocompatibility, ACS Nano 6 (2012) 7340–7351.
[5] P. Xu, E.A. Van Kirk, Y. Zhan, W.J. Murdoch, M. Radosz, Y. Shen, Targeted charge–reversal nanoparticles for nuclear drug delivery, Angew. Chem. Int. Ed. 46 (2007) 4999–5002.
[6] M. Narvekar, H.Y. Xue, J.Y. Eoh, H.L. Wong, Nanocarrier for poorly water-soluble anticancer drugs — barriers of translation and solutions, AAPS PharmSciTech 15 (4) (2014) 822–833.
[7] M.M. Yallapu, F.S. Othman, E.T. Curtis, B.K. Gupta, M. Jaggi, S.C. Chauhan, Multifunctional magnetic nanoparticles for magnetic resonance imaging and cancer therapy, Biomaterials 32 (2011) 1890–1905.
[8] A. Babul Reddy, B. Manjula, T. Jayaramudu, E.R. Sadiku, P. Anand Babu, S. Periyar Selvam, 5-Fluorouracil loaded chitosan–PVA/Na^+MMT nanocomposite films for drug release and antimicrobial activity, Nano-Micro Lett. 8 (3) (2016) 260–269.
[9] A.P. Majewski, A. Schallon, V. Jerome, R. Freitag, A.H.E. Muller, H. Schmalz, Dual-responsive magnetic Core–Shell nanoparticles for nonviral gene delivery and cell separation, Biomacromolecules 13 (2012) 857–866.
[10] N. Chan, M. Laprise-Pelletier, P. Chevallier, A. Bianchi, M.-A. Fortin, J.K.J. Oh, Multidentate block-Copolymer-Stabilized ultrasmall superparamagnetic iron oxide nanoparticles with enhanced colloidal stability for magnetic resonance imaging, Biomacromolecules 15 (2014) 2146–2156.
[11] N.D. Thorat, S.V. Otari, R.A. Bohara, H.M. Yadav, V.M. Khot, A.B. Salunkhe, M.R. Phdatre, A.I. Prasad, R.S. Ningthoujam, S.H. Pawar, Structured super-paramagnetic nanoparticles for high performance mediator of magnetic fluid hyperthermia: synthesis, colloidal stability and biocompatibility evaluation, Mater. Sci. Eng. C 42 (2014) 637–646.
[12] D.A. Cameron, H. Gabra, R.C. Leonard, Continuous 5-fluorouracil in the treatment of breast cancer, Br. J. Cancer 70 (1) (1994) 120–124.
[13] E. Healey, G.E. Stillfried, S. Eckermann, J.P. Dawber, P.R. Clingan, M. Ranson, Comparative effectiveness of 5-fluorouracil with and without oxaliplatin in the treatment of colorectal cancer in clinical practice, Anticancer Res. 33 (3) (2013) 1053–1060.
[14] H. Chen, W. Wu, Y. Li, T. Gong, X. Sun, Z. Zhang, A novel brain targeted 5-FU derivative with potential antitumor efficiency and decreased acute toxicity: synthesis, in vitro and in vivo evaluation, Die Pharmazie 69 (4) (2014) 271–276.
[15] M. Osaki, S. Tatebe, A. Goto, H. Hayashi, M. Oshimura, H. Ito, 5-fluorouracil (5-FU) induced apoptosis in gastric cancer cell lines: role of the p53 gene, Apoptosis 2 (2) (1997) 221–226.
[16] N.G. Shishu, A. Nidhi, Stomach-specific drug delivery of 5-fluorouracil using floating alginate beads, AAPS PharmSciTech 8 (2) (2007) E143–E149.
[17] S. Li, A. Wang, W. Jiang, Z. Guan, Pharmacokinetic characteristics and anticancer effects of 5-fluorouracil loaded nanoparticles, BMC Cancer 8 (2008) 103.
[18] K. Kavitha, R.A. Srinivasa, C.N. Nalini, An investigation on enhancement of solubility of 5-fluorouracil by applying complexation technique characterisation, dissolution and molecular modelling studies, J. Appl. Pharm. Sci. 3 (2013) 162–166.
[19] C.O. Ehi-Eromosele, B.I. Ita, E.E.J. Iweala, K.O. Ogunniran, J.A. Adekoya, F.E. Ehi-Eromosele, Structural and magnetic characterization of la0. 7Sr0. 3MnO3 nanoparticles obtained by the citrate-gel combustion method: effect of fuel to oxidizer ratio, Ceram. Int. 42 (2016) 636–643.
[20] W. Stober, A. Fink, E. Bohn, Controlled growth of monodisperse silica spheres in micron size range, J. Colloid Interface Sci. 26 (1968) 62–69.
[21] K.P. Sonu, Nobel Metal Nanostructures: Synthesis and Modification for Biomedical Applications, M.Sc Thesis Submitted to ICMS, Jawarharlal Nehru Center for Advanced Scientific Research, Bangalore, India, 2014.
[22] M.Y.K. Vimala, K. Varaprasad, N. Reddy, S. Ravindra, N. Naidu, K. Raju, Fabrication of curcumin encapsulated chitosan–PVA silver nanocomposite films for improved antimicrobial activity, J. Biomater. Nanobiotechnol. 2 (2011) 55–64.
[23] V. Uskokovic, A. Kosak, M. Drofenik, Preparation of silica-coated lanthanum strontium manganite particles with designable curie point for application in hyperthermia treatments, Int. J. Appl. Ceram. Technol. 3 (2) (2006) 134–143.
[24] J. Choi, J.C. Kim, Y.B. Lee, I.S. Kim, Y.K. Park, N.H. Hur, Fabrication of silica-coated magnetic nanoparticles with highly photoluminescent lanthanide probes, Chem. Commun. 16 (2007) 1644–1646.
[25] A.T. Raghavender, Synthesis and characterization of cobalt ferrite nanoparticles, Sci. Tech. Arts Res. J. 2 (2013) 01–04.
[26] A.B. Salunkhe, V.M. Khot, N.D. Thorat, M.R. Phadatare, C.I. Sathish, D.S. Dhawale, S.H. Pawar, Polyvinyl alcohol functionalized cobalt ferrite nanoparticles for biomedical applications, Appl. Surf. Sci. 264 (2013) 598–604.
[27] S.A. Shah, M.H. Asdi, M.U. Hashmi, M.F. Umar, S. Awan, Thermoresponsive co-polymer coated $MnFe_2O_4$ magnetic nanoparticles for hyperthermia therapy and controlled drug delivery, Mater. Chem. Phys. 137 (2012) 365–371.
[28] F. Gao, R.A. Lewis, X.L. Wang, S.X. Dou, Far-infrared reflection and transmission of $La_{1-x}Ca_xMnO_3$, J. Alloys Compd. 347 (2002) 314–318.

[29] D.A. Macedo, M.R. Cesário, G.L. Souza, B. Cela, C.A. Paskocimas, A.E. Martinelli, D.A. Melo, R.M. Nascimento, Infrared spectroscopy techniques in the characterization of SOFC functional ceramics, in: Theophanides Theophile (Ed.), Infrared Spectroscopy Materials Science, Engineering and Technology, InTech, 2012, pp. 304–404.
[30] R.A. Vargas, R. Chiba, M. Andreoli, E.S.M. Seo, Synthesis and characterization of $La_{1-x}Sr_xMnO_{3\pm\delta}$ and $La_{1-x}Sr_xCo_{1-y}Fe_yO_{3-\delta}$ used as cathode in solid oxide fuel cells, Cerâmica 54 (2008) 366–372.
[31] A. Bertoluzza, C. Fagnano, M.A. Morelli, V. Gottardi, M. Guglielni, Raman and infrared spectra on silica gel evolving toward glass, J. Non Cryst. Solids 48 (1982) 117–128.
[32] M.C. Matos, L.M. Iiharco, R.M. Almeida, The evolution of TEOS to silica gel and glass by vibrational spectroscopy, J. Non-Cryst. Solids 147 (1992) 232–237.
[33] H. Yoshino, K. Kamiya, H. Nasu, IR study on the structural evolution of sol gel derived SiO_2 gels in the early stage of conversion to glasses, J. Non-Cryst. Solids 126 (1990) 68–78.
[34] X. Xiao, K. Huang, Q. He, Synthesis and characterization of aminated $SiO_2/CoFe_2O_4$ nanoparticles, Trans. Non-ferrous Met. Soc. China 17 (2007) 118–1122.
[35] R. Scaffaro, L. Botta, G.L. Re, R. Bertani, R. Milani, A. Sassi, Surface modification of poly(ethylene- co-acrylic acid) with amino-functionalized silica nanoparticles, J. Mater. Chem. 21 (2011) 3849–3857.
[36] M.J. Meziani, J. Zajac, D.J. Jones, J. Roziere, S. Partyka, Surface characterisation of mesoporous silicoaluminates of the MCM-41 type: evaluation of polar surface sites using flow calorimetry, adsorption of a cationic surfactant as a function of pore size and aluminium content, Langmuir 13 (1997) 5409–5417.
[37] Y.-J. Lu, K.C. Wei, C.M. Ma, S.-Y. Yang, J.-P.Y.-J. Chen, Dual targeted delivery of doxorubicin to cancer cells using folate-conjugated magnetic multi-walled carbon nanotubes, Colloids Surf. B: Biointerfaces 89 (2012) 1–9.